Pattern Recognition 48 (2015) 2725–2737

Contents lists available at ScienceDirect

Pattern Recognition

journal homepage: www.elsevier.com/locate/pr

Subject-dependent classification for robust idle state detection using multi-modal neuroimaging and data-fusion techniques in BCI ☆

Min-Ho Lee [a], Siamac Fazli [a], Jan Mehnert [b], Seong-Whan Lee [a,*]

[a] Department of Brain and Cognitive Engineering, Korea University, Anam-dong, Seongbuk-ku, Seoul 136-713, Korea
[b] Department of Computer Science, Berlin Institute of Technology, Germany

ARTICLE INFO

Article history:
Received 23 May 2014
Received in revised form
30 December 2014
Accepted 8 March 2015
Available online 18 March 2015

Keywords:
Hybrid brain–computer interfacing
Combined EEG–NIRS
Classifier combination
Subject-dependent classification

ABSTRACT

Brain–computer interfaces (BCIs) allow users to control external devices by their intentions. Currently, most BCI systems are synchronous. They rely on cues or tasks to which a subject has to react. In order to design an asynchronous BCI one needs to be able to robustly detect an idle class. In this study, we examine whether multi-modal neuroimaging, based on simultaneous EEG and near-infrared spectroscopy (NIRS) measurements, can assist in the robust detection of the idle class within a sensory motor rhythm-based BCI paradigm. We propose two types of subject-dependent classification strategies to combine the information of both modalities. Our results demonstrate that not only idle-state decoding can be significantly improved by exploiting the complementary information of multi-modal recordings, but also it is possible to minimize the delay of the system, caused by the slow inherent hemodynamic response of the NIRS signal.

1. Introduction

Brain–computer interface (BCI) systems have been developed to allow users to control computers or external devices using their intentions, which are decoded from their brain activity [2,3]. The majority of sensory motor rhythm (SMR)-based BCIs require the subject to react to a cue from the device, known as a cue-paced or synchronous BCI. However, synchronous BCI systems are disadvantageous for a broad range of applications outside the laboratory, such as wheel-chair operation [4] and various other rehabilitation devices [5]. Therefore, it is necessary to design stable BCI systems with the capability of detecting asynchronous (or self-paced) actions of a subject.

In asynchronous BCI paradigms the users' intentions are divided into *active* and *idle states*. During the *active state* the user concentrates on the specific mental tasks to operate the system. During the idle state the subject is not required to interact with the system. The robust detection of idle states is highly important for the successful operation of asynchronous BCIs. To date, a number of classification strategies have been proposed for this purpose. Power et al. [6] propose a one-vs-rest (OVR) classifier, system-paced NIRS-BCI which detects an idle state as well as two active states, corresponding to either mental arithmetic or mental singing. Zhang et al. [7] designed an EEG-based, two-stage system of two binary classifiers, where the first stage binary classifier decodes idle and active states. Once an active state is detected, the second binary classifier is used to identify the active class. Millán and Mouriño [8] propose an EEG-based, one direction wheelchair operation system, which activates with a foot imagery task. The system activates when the bandpower of EEG signals exceed a subject-dependent threshold.

Enhancing the accuracy and universality of BCI decoding are priorities of current BCI research. Therefore various types of optimization techniques [9,10] and paradigms [11] have been proposed to improve BCI performance and universality. One solution of stabilizing the outcome of BCIs lies in using two or more modalities of neuroimaging data, i.e., measurement devices forming a *hybrid BCI* [1,12,13].

Fazli et al. [14] proposed a hybrid sensory motor rhythm (SMR)-based BCI paradigm combining NIRS and EEG. A meta-classifier is constructed to combine the classifier outputs of the individual modalities. Classification performances of unimodal EEG and NIRS as well as multi-modal EEG+NIRS are compared. Their results show that simultaneous measurements of NIRS and EEG can significantly improve the classification accuracy of motor imagery in over 90% of considered subjects and lead to performance increases of 5% on average.

While EEG, the most commonly used device in the context of non-invasive BCIs, measures scalp voltage fluctuations, which result from ionic current flows of the neuronal activity, NIRS

☆A preliminary partial version of this work was presented at the 2nd Asian Conference on Pattern Recognition, Okinawa, Japan, November 2013 [1].

* Corresponding author. Tel.: +82 2 3290 3197; fax: +82 2 3290 3583.
E-mail addresses: mh_lee@korea.ac.kr (M.-H. Lee), fazli@korea.ac.kr (S. Fazli), jan@mehnert.org (J. Mehnert), sw.lee@korea.ac.kr (S.-W. Lee).

http://dx.doi.org/10.1016/j.patcog.2015.03.010
0031-3203/

(like fMRI) depends on focal changes in cerebral blood flow, i.e. on concentration changes of the chromophores deoxygenated and oxygenated hemoglobin following neuronal activity [15]. Previous NIRS and fMRI studies reported a peak of the hemodynamic response with a delay of approximately 6 s after stimulus onset [16]. Because of the temporal resolution of the hemodynamic response, previous NIRS studies were designed as synchronous paradigms with relatively long task periods of more than 10 s for motor [17], cognitive [18] among others.

However, in a real-time asynchronous setting, it would be inconvenient to wait for 6 s after a mental command. Furthermore, Information Transfer Rates (ITRs) would be greatly impaired by doing so. Therefore, the hemodynamic response delay is the primary limitation preventing NIRS from real-time BCI applications. This limited responsiveness results in decreased usability of the system and can therefore not be seen as a viable alternative to EEG-based BCI's, which can usually be operated in real-time. In summary, an EEG–NIRS hybrid system should not only improve the classification performance but should also maintain a reasonable ITR for the purpose of real-world BCI applications.

In this study, we propose to leverage the temporal dynamics of the output of a NIRS-based classifier that distinguishes the idle state from active states (formerly termed *brain switch* [19]). The extremes of the classifier output indicate the transitions of mental states even before the peak of the hemodynamic response is reached; therefore, we are able to circumvent this time delay to some degree.

Previous multi-modal studies have shown a high variability between NIRS and EEG classification accuracies for single subjects [14]. This indicates that each modality is not contributing equally to the classification, even though the neuronal signals are extracted simultaneously from same subject. Therefore, novel classification and data-fusion strategies of using EEG and NIRS signals are needed for hybrid EEG–NIRS systems. While a complete review of this topic is beyond the scope of this paper (for further reading, refer to [20]), here we will outline two recent developments, namely temporal kernel Canonical Correlation Analysis (tkCCA) [21] and multimodal source power correlation analysis (mSPoC) [22]. While tkCCA is a multivariate extension of the crosscorrelogram between data sources that have different dimensionalities and temporal resolutions, mSPoC maximizes the correlation of two raw multimodal multivariate signals that are spatially and temporally sampled differently and are coupled through a nonlinear transformation. In this paper we propose two distinct subject-dependent classification strategies based on unimodal EEG and NIRS classifiers.

The real-time feedback data in this study was originally recorded with a cue-based paradigm. However, this paradigm combines short task periods with long idle periods, such that it enabled us to test whether our proposed method can be extended for an asynchronous BCI setting in the future. Our results not only demonstrate that idle as well as active state decoding can be significantly improved by exploiting the complementary information of multi-modal recordings, but also that it is possible to somewhat minimize the system response, caused by the inherent hemodynamic delay of the NIRS signal.

2. Methods

2.1. Experimental setup

2.1.1. Participants and experimental paradigm

In order to find out whether the multi-modal setup can assist in improving the accuracy of the idle-state detection we used data from a previous study [14]. While this study was recorded in a synchronous manner, there were relatively long 'no-task' periods, which were used to estimate and validate our proposed method. In this study 14 healthy, right-handed volunteers (aged 20–30) participated. The subjects were seated in a comfortable chair with armrests and were instructed to relax their arms. The experiment considered here consisted of 2 sessions of motor imagery with visual feedback. Each session consists of 50 trials of right hand and 50 trials of left hand imagery tasks (100 trials per session). For all blocks the first 2 s of each trial began with a black fixation cross that appeared at the center of the screen. Then, an arrow appeared as a visual cue and pointing to the left or right. During the motor imagery the fixation cross started moving for 4 s, according to the real-time classifier output of the EEG signal. After 4 s the cross disappeared and the screen remained blank for 10.5 ± 1.5 s. The online processing was based on the concept of co-adaptive calibration [23] and details are described in the Data analysis section.

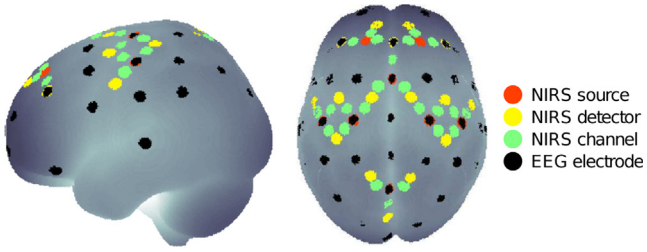

Fig. 1. Setup of NIRS sources and detectors and EEG electrodes.

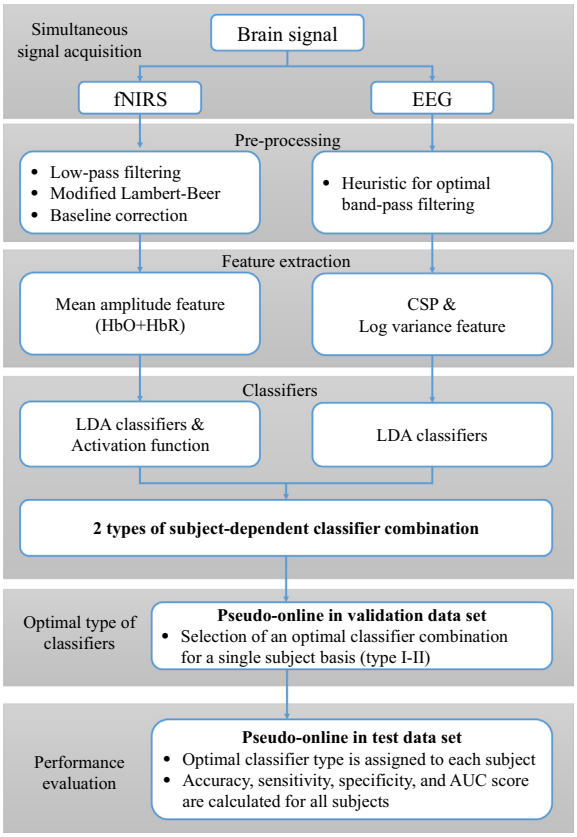

Fig. 2. The flowchart of data analysis of simultaneous EEG and fNIRS brain signals for the pseudo-online BCI system. The steps of pre-processing, feature extraction and classifiers were separately applied to each signals. Also the classification accuracies were estimated in the validate data set to find the optimal classifier set for each subjects. Finally, the test data set was used for estimation of the performance.

2.1.2. Data acquisition

During the experiment, simultaneous EEG and NIRS brain signals were recorded. The NIRS-System (NIRScout 8-16, NIRx Medizintechnik GmbH, Germany) was equipped with 24 optical fibers (8 sources with wavelength of 760 nm and 850 nm, 16 detectors convolving to 24 measurement channels) and fixated on the subject's head with inter-optode distances between 2 and 3 cm. The sampling frequency of the NIRS was $f_{NIRS} = 6.25$ Hz. EEG signals were recorded with a multichannel EEG amplifier (BrainAmp by Brain Products, Munich, Germany) using 37 Ag/AgCl electrodes at a sampling frequency of $f_{EEG} = 1$ KHz and then down sampled to 100 Hz. EEG electrodes and the optical probes (sources and detectors) were located according to the international 10–20 system and covered frontal, motor and parietal areas of the head as shown in Fig. 1. Most NIRS probes shared their position with electrodes, allowing us to extract neuronal and hemodynamic brain signals from the same cortical areas.

2.2. Data analysis

Fig. 2 shows a flow chart of EEG–NIRS data analysis. EEG and NIRS signals were analyzed separately as part of preprocessing and feature extraction. We then introduce two types of subject-dependent classifier combinations and optimal type selection algorithm. The specific steps of data analysis are described below.

2.2.1. Preprocessing

Raw NIRS data (attenuation changes) was transformed to hemoglobin concentration (oxygenated (HbO) and deoxygenated (HbR) hemoglobin) changes with a modified Beer–Lambert law (differential path length factors: 5.98 (for higher wavelength: 830 nm) and 7.15 (for lower wavelength: 760 nm)) [24]. Then, NIRS data was low-pass filtered at 0.2 Hz using a one-directional digital filter, namely a 3rd order Butterworth-filter.

From both EEG and NIRS, 50 trials of each task (right and left hand imagery) and 100 trials of idle state data (i.e., data in between the actual trials) were segmented within each of the 2 experimental sessions (accumulating into 100 trials of imagery tasks and 100 trials of idle state per session). The whole first session was used as training data, while the second session was further split into two equal parts: half of the data were used as the validation set and half as the test set. The data of the first session (i.e. the training data) was used to estimate all classifiers for NIRS and EEG. The validation set was used to find the optimal classifier type for each subject (as will be explained in Section 2.2.5). Finally, the test data was employed for the final performance evaluation.

Table 1
Binary single-trial classification accuracies (%) of uni-modal imaging, i.e. either EEG or NIRS for the individual subjects, as well as their mean. For EEG all binary combinations of one particular class versus all other classes are considered, as well as 'L vs. R', where 'L' and 'R' stand for left and right hand imagery, respectively. For NIRS only the classification accuracy of the idle class versus all other classes is considered for the individual chromophores as well as their combination.

Subject	EEG				NIRS		
	R vs. others	L vs. others	Idle vs. others	R vs. L	Idle vs. others (HbO)	Idle vs. others (HbR)	Idle vs. others (Comb)
a	65.9	71.5	72.6	47.6	91.1	91.9	93.9
b	97.5	98.2	94.0	99.0	80.1	78.0	87.4
c	70.2	77.0	72.9	69.3	59.7	64.6	72.1
d	80.4	88.1	97.9	78.3	88.9	87.5	87.2
e	79.9	74.0	95.8	86.0	87.1	90.9	90.3
f	70.9	73.0	69.3	64.5	72.6	60.6	79.7
g	91.4	88.0	93.8	85.6	91.1	90.0	91.3
h	88.1	92.0	88.9	92.4	84.3	87.1	92.5
i	66.0	65.3	60.8	57.4	65.2	71.9	78.6
j	81.2	87.6	77.0	91.0	86.4	74.6	87.7
k	90.6	90.2	77.6	98.0	95.8	91.5	93.0
l	95.5	97.0	91.0	98.2	96.6	99.2	97.8
m	67.9	71.0	85.5	63.3	81.1	72.0	81.9
n	96.9	97.4	95.0	98.6	94.9	90.5	95.7
Mean	81.6	83.6	83.7	80.7	83.9	82.2	87.8

2.2.2. Feature extraction and classification

For the EEG data, we consider two different analysis methods. A common approach in sensory-motor rhythm based BCI research is to estimate subject-dependent band-pass filters from training data with a established heuristic [25]. This heuristic depends on the Laplacian spatial filter to reduce the volume conduction effects in the EEG signals [26]. After applying the temporal filter to the data, Common Spatial Patterns (CSP) were used as spatial filters [27]. Log-variances of the temporally and spatially filtered data were calculated as features. We also applied a novel Bayesian framework for discriminative feature extraction, which was developed for binary motor imagery classification. Here the class-discriminative frequency bands and the corresponding spatial filters are optimized by means of a probabilistic and information-theoretic approach. The method is termed Bayesian spatiospectral filter optimization (BSSFO) and has shown to outperform a number of competing algorithms, such as CSSP, FBCSP among others [9]. For further details on the theory and implementation, refer to [28].

For the NIRS signal, a baseline correction was performed by subtracting the average from -2 s to 0 s before stimulus onset from each trial. Then, features were calculated as mean amplitudes of the hemodynamic changes of HbO as well as HbR, in the interval between 4 s and 6 s with respect to stimulus onset.

Linear Discriminant Analysis (LDA) is a technique for pattern recognition that finds linear combinations of features to separate the classes by maximizing between-class variance, while minimizing within-class variance [29]. The projection matrix maximizes the ratio of the determinant defined by Eq. (1), where $\mathbf{S_B}$ and $\mathbf{S_W}$ denote the between-class and within-class covariance matrices, respectively and $\mathbf{w}$ the hyper-plane for separation of the classes, which can be obtained by maximizing the Rayleigh coefficient:

$$\mathbf{w} = \arg\max_{\mathbf{w}} \frac{\mathbf{w}^T \mathbf{S_B} \mathbf{w}}{\mathbf{w}^T \mathbf{S_W} \mathbf{w}} \tag{1}$$

To separate the three classes (left hand imagery, right hand imagery, and idle) two classification strategies, namely *One Versus the Rest* (*OVR*) and *Within the Binary* (*IN*) were considered (see [30,31] for further details). The following *OVR* classifiers and CSP filters were estimated for EEG: *left vs. others*, *right vs. others* and *idle vs. others*. Only one *IN* LDA classifier and CSP filter was estimated for EEG: *left vs. right* (see Algorithm 1). Three *OVR* classifiers were estimated for NIRS (Idle-state detector): *idle vs. others* (HbO), *idle vs. others* (HbR) and *idle vs. others* (HbO and HbR, concatenated). Therefore, four LDA parameters: $(w_j, b_j)_{j=1,2,3,4}$ and CSP spatial filters were calculated for EEG signals, and three LDA parameters were calculated for the NIRS signal: $(w_j, b_j)_{j=5,6,7}$ on the training data. Binary single-trials classification accuracies for all type of classifier were evaluated based on 10-fold cross validation. Results of the NIRS classification indicated best performance for the combination of HbO and HbR features (see Table 1). Therefore, the combination of HbO and HbR was chosen for the idle-state detector in the further analysis.

Algorithm 1. Subject-dependent classifier algorithm.

Input: A set of training data $\{\mathbf{X},\mathbf{\Omega}\},\{\mathbf{Y},\mathbf{\Omega}\}$.

- $\mathbf{X}=\{x_j^i\}_{i=1}^{D}, x_j^i \in \mathbb{R}^{N\times T}$: a set of single-trial EEG for each type of data, where D is the total number of trials with N channels and T sample points.
- $\mathbf{Y}=\{y_j^i\}_{i=1}^{D}, y_j^i \in \mathbb{R}^{N\times T}$: a set of single-trial NIRS for [HbO] and [HbR], where D is the total number of trials with N channels and T sample points.
- $\mathbf{\Omega}=\{\omega_j^i\}_{i=1}^{D}$: corresponding class labels for types of data, where $\omega_i \in \{+1,0,-1\}$.
- $S=\{1,2,3,4,5\}$: type of data set represents the $EEG_{\text{right vs. others}}$, $EEG_{\text{left vs. others}}$, $EEG_{\text{idle vs. others}}$, $EEG_{\text{right vs. left}}$, $NIRS_{\text{idle vs. others}}$.

Output: A set of LDA parameters and the spatial filters.

- $\mathbf{P}=\{w_j,b_j\}_{j=S_1}^{S_5}$: a set of LDA parameters, where w and b denote transformation matrix and bias.
- $\mathbf{W}=\left\{\hat{W}\right\}_{j=S_1}^{S_4}$: a set of spatial filters for EEG data.

Training classifier:

for $j=S_1$ **to** S_4 **do**
  $\mathbf{Z}_j=B\bigotimes\mathbf{X}$ ▷ B=bandpass filter, $\mathbf{Z}_j=\{\mathbf{z}_j^i\}_{i=1}^{D}$
  Solve $W^{-1}(\Sigma^{(+)}+\Sigma^{(-)})W=I$ ▷ Perform a CSP algorithm
  $\hat{W}_j$= the first m and the last m column vectors in W
  for i=1 **to** D **do**
    $f_j^i=\log[\mathrm{var}(\hat{W}_j\mathbf{z}_j^i)]$ ▷ Feature extraction, $\mathbf{F}_j=\{f_j^i\}_{i=1}^{D}$
  end
  $(w_j,b_j)=LDA(\mathbf{F}_j,\mathbf{\Omega})$ ▷ EEG LDA parameters
end
$j=S_5$
for i=1 **to** D **do**
  $\text{baseline}_j^i=\frac{1}{\tau}\sum_{t=1}^{\tau}\mathbf{Y}_t$
  $\mathbf{Y}'=\mathbf{Y}-\text{baseline}_j^i$
  $f_j^i=\frac{1}{n2-n1}\sum_{t=n1}^{n2}\mathbf{Y}'_t$ ▷ Feature extraction, $\mathbf{F}_j=\{f_j^i\}_{i=1}^{D}$
end
$(w_j,b_j)=LDA(\mathbf{F}_j,\mathbf{\Omega})$ ▷ NIRS LDA parameters

2.2.3. Pseudo-online emulation

To emulate a classification in real-time, the classifiers were fed with data from a moving window (width=1 s, step size=0.5 s). This procedure emulates a pseudo-online asynchronous paradigm [32]. Given a LDA hyper-plane formulation (w^TX+b), continuous LDA outputs are obtained from EEG as well as from NIRS data. X ($X\in\mathbb{R}^{N_E\times T_E}$) and Y ($Y\in\mathbb{R}^{N_N\times T_N}$) denote continuous EEG and NIRS data, respectively, with N_E and N_N denoting the number of channels and T_E and T_N sample points for EEG and NIRS, respectively. Finally, j represents the selected classifier and k the index of the moving window:

$$p_j^k=(w_j)^TX_k+b_j,\quad j=1,2,3,4 \tag{2}$$

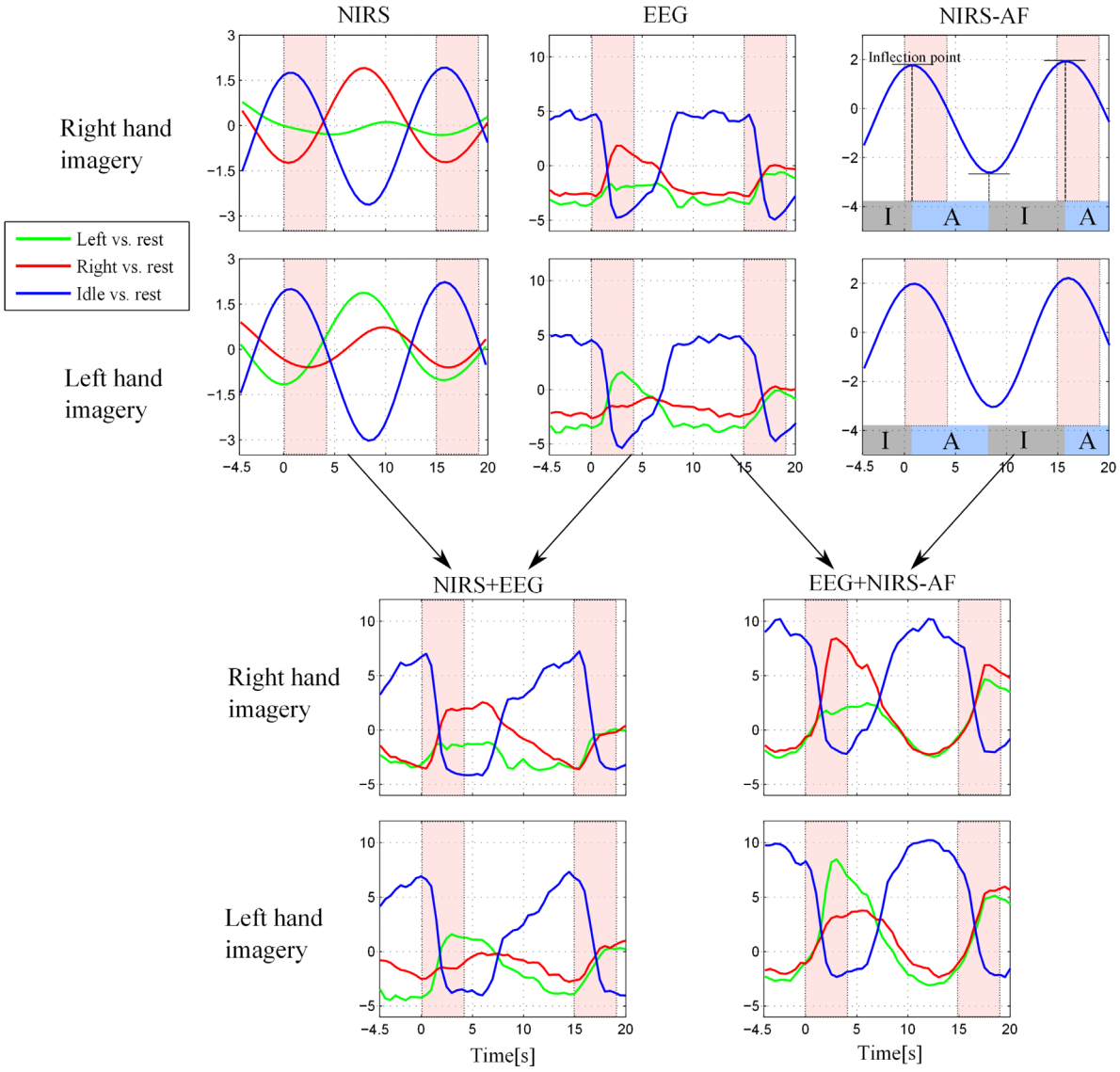

Fig. 3. Upper rows show grand average NIRS and EEG LDA outputs for three OVR classifiers. The right panel shows the activation, derived from the 'Idle vs. others' NIRS classifier. The first column of the lower panels depicts the combination of NIRS and EEG classifier outputs, while the second column depicts the combination of EEG with the NIRS activation function (type II). Highlighted areas indicate the onset and offset of an active trial (i.e. right or left hand imagery). The first red highlighted area marks a right/left (top/bottom) hand imagery trial while the second one marks the onset of the next motor imagery trial (which could be either left or right hand imagery). (For interpretation of the references to color in this figure caption, the reader is referred to the web version of this paper.)

$$p_5^k = (w_j)^T Y_k + b_j, \quad j = 7 \tag{3}$$

2.2.4. *Activation function*

OVR-based LDA outputs are calculated using the time series of EEG and NIRS data. The continuous LDA output is then segmented by the stimulus onset of each class (right and left hand imagery movements) and averaged. As can be seen in the top-middle part of Fig. 3, the EEG classifier outputs for the active classes (red and green lines) show an immediate increase, shortly after stimulus onset, while the blue line (idle class) decreases.

However, a delayed response can be observed (see left part of Fig. 3) in the classes of the NIRS classifier output. This delay is caused by the slow hemodynamic response (see Section 1). Here we propose a NIRS-based activation function (formerly termed *brain switch* [19]) to distinguish between active and idle brain states. The activation function consists of a binary (0 or 1) number, signifying either an active or an idle mental state. It is derived from the continuous 'idle vs. others' NIRS-derived classifier output (p_7^k). Inflection points on this curve, i.e., where the curvature changes its sign from plus to minus (or from minus to plus), are considered a change in the subject's current mental state (from idle to active, or vice versa). The activation function is then set to 1 (or 0) as can be seen in Fig. 4(a). The lower left columns of Fig. 3 depicts the sum of NIRS and EEG classifier outputs on a single-trial basis. The lower right column depicts the combination of EEG and NIRS with the help of an activation function. The details of how this is performed are given in the next section.

2.2.5. *Optimal combination of classifiers*

To estimate the three mental states (right, left, and idle), we propose and examine two distinct subject-dependent classification strategies for combining EEG and NIRS using EEG classifiers and NIRS-based activation function. The first approach (type I) is to use the activation function to determine whether a subject is in an *active* or *idle* mental state. If an *active state* is detected by the activation function, the binary right vs. left EEG classifier output (p_4^k) is

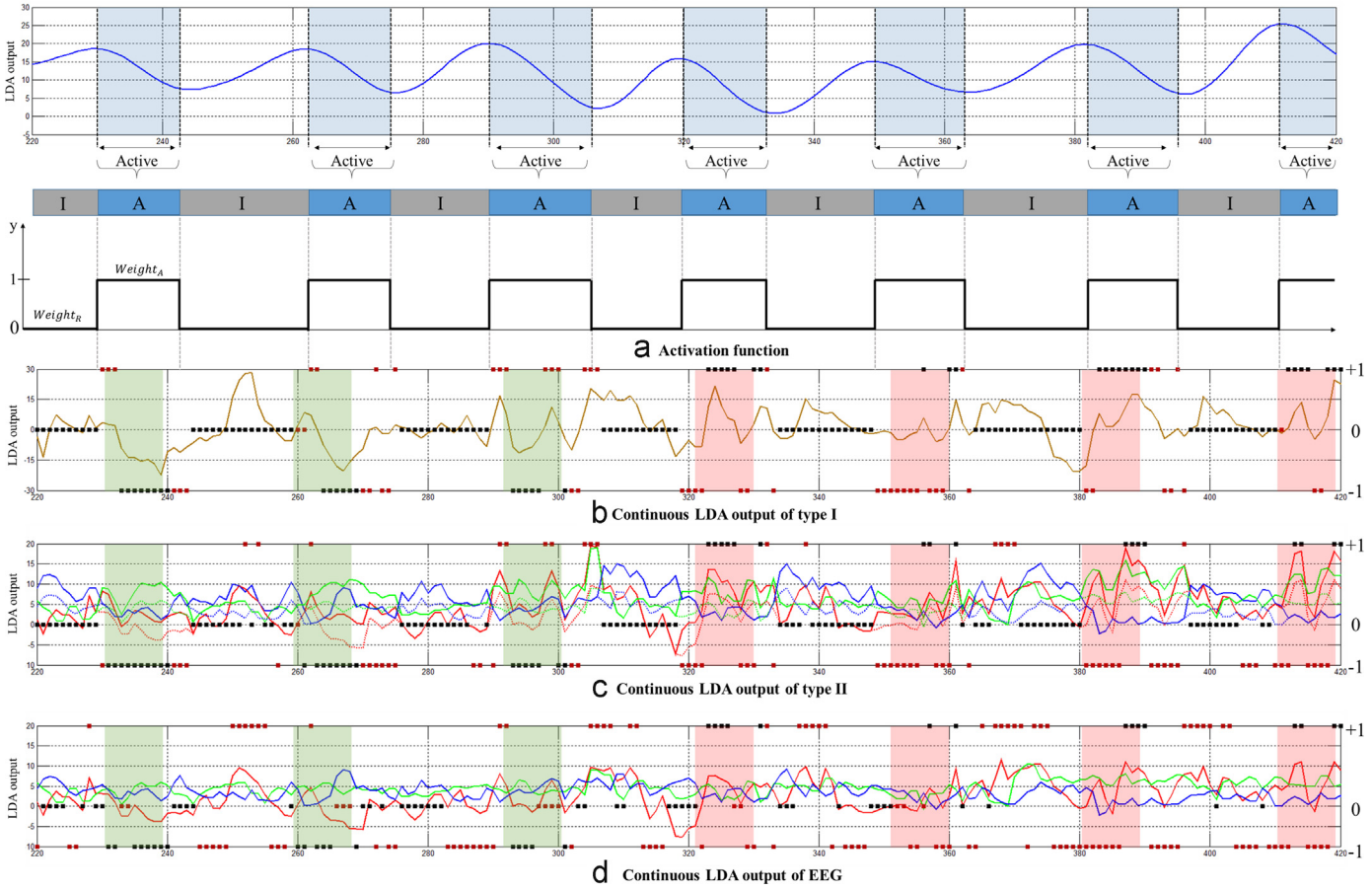

Fig. 4. (a) Activation function and the classification outputs of the proposed two types of classifier combinations for roughly 2 min of the experiment. (b) Type I – when the activation function predicts an active state, a binary EEG classifier (yellow line) is used to determine the active class (i.e. right or left hand imagery). (c) Type II – the activation function is used for weighting the three EEG classifier outputs. (d) Original EEG classifier outputs are shown. The red and green patches indicate the true active classes (red: right hand imagery, green: left hand imagery) as well as their duration. Square boxes indicate the systems outputs. Red boxes mark incorrect outputs, while black boxes indicate correct outputs. (For interpretation of the references to color in this figure caption, the reader is referred to the web version of this paper.)

employed to decode the direction of the imagery movement:

$$y^k = \begin{cases} \mathrm{sgn}(p_4^k) & \text{if } \psi^k = 1, \\ 0, & \text{if } \psi^k = 0, \end{cases} \tag{4}$$

where ψ^k denotes the activation function and $y^k \in \{-1, 0, +1\}$ the estimated classifier output corresponding to right, idle and left class, respectively (see Fig. 4(b)).

The second approach of combining the individual classifiers estimates the current mental state ('left' or 'right' hand imagery or 'idle') on the basis of the three OVR-based EEG classifiers described in Section 2.2.2. The activation function is used to weight the output of each of the three EEG classifiers. To further illustrate, when the NIRS-based activation function is 1 (active state), the outputs of the EEG-based classifiers containing an active classes (corresponding to $EEG_{\text{right vs. others}}$ and $EEG_{\text{left vs. others}}$) are raised. Conversely, when the activation function is 0 (idle state), the output of the EEG-based classifier containing the idle class (corresponding to $EEG_{\text{idle vs. others}}$) is raised:

$$p'^k_{j,j\in\{1,2,3\}} = \begin{cases} p^k_{1,2} + \alpha_k & \text{if } \psi^k = 1 \\ p^k_3 + \alpha_k & \text{if } \psi^k = 0 \end{cases} \tag{5}$$

where j ($j \in \{1, 2, 3\}$) denotes the classifier index as described in Section 2.2.3 and ψ^k denotes the kth value of the activation function. α denotes the weight value by considering the distribution of three classifiers output with optimal parameter θ.

The maximum output of the three OVR classifiers is determined as the current predicted mental state. In order to find the optimal weighting parameter for each subject, a grid search was performed on the validation data set using Area under the Receiver Operating Curve (AUC) as a loss function:

$$y^k = \arg\max_j \left(p'^k_j\right) \tag{6}$$

$$\theta^* = \arg\max_\theta \left(AUC(y^k, Y^k)\right) \tag{7}$$

where y^k denotes the estimated label, Y^k the true label and θ^* the optimal weighting parameter. The parameters of θ were varied between 0.1 and 3 on a linear scale. The optimal parameter θ which has shown the peak of AUC score is selected across all subjects as can be seen in Fig. 7.

To determine which of the proposed classifier combinations (i.e., type I–II) is optimal for a given subject, type with the maximum AUC score is selected. Finally, the optimal type is applied to the test data of the individual subjects. The exact algorithm is presented in Algorithm 2.

Algorithm 2. Subject-dependent classifier algorithm (cont.)

Input: A set of validate data $\{\mathbb{X}, \mathbf{\Omega}'\}, \{\mathbb{Y}, \mathbf{\Omega}'\}$.

- $\mathbb{X} \in \mathbb{R}^{\mathbf{N}\times\mathbf{T}}$: Continuous EEG data with N channels and T sample points.
- $\mathbb{Y} \in \mathbb{R}^{\mathbf{N}\times\mathbf{T}}$: Continuous NIRS data with N channels and T sample points.
- $\mathbf{\Omega}' \in \{+1, 0, -1\}$: corresponding class labels.

Output: An optimal type of classifier combination and weight-parameter for a single subject.

Optimization:

for k=*1* **to** K **do**
  $\mathbf{Z}_k = B \bigotimes \mathbb{X}_{\mathbf{k}}$
  for $j = S_1$ **to** S_4 **do**
    $f_k^j = \log[\mathrm{var}(\hat{W}_j \mathbf{Z}_k)]$ ▷ EEG: Log variance feature
    $p_k^j = (w_j)^T f_k^j + b_j$
  end
  $j = S_5$
  $g_k = \bar{\mathbb{Y}}_k$ ▷ NIRS: Mean feature
  $p_k^j = (w_j)^T g_k^j + b_j$
  $\psi_k = \mathrm{Active}\left(p_k^j\right)$
end
for θ=*0.1* **to** 3 **do**
  for k=*1* **to** K **do**
    $\alpha_k = \theta\left(\frac{1}{S_3}\sum_{j=S_1}^{S_3}\left|p_k^j\right|\right)$
    $p'^k_j = \begin{cases} \alpha_k + p^k_{j=S_1,S_2} & \text{if, } \psi^k = 1 \\ \alpha_k + p^k_{j=S_3}, & \text{if, } \psi^k = 0 \end{cases}$
  end
  $P_\theta^k = \arg\max_j\left(p'^k_j\right)$
end
$Y_n^k = \begin{cases} sgn(p'^k_4) & \text{if, } \psi^k = 1, \\ 0, & \text{if, } \psi^k = 0, \end{cases}$ ▷ Type I
$Y_{n+1}^k = \arg\max_\theta\left(P_\theta^k\right)$ ▷ Type II
$\mathrm{Type} = \arg\max_n\left(AUC(Y_n^k, \Omega')\right)$

Fig. 4 shows a sketch of how the proposed classifier combinations are applied practically. On the top of Fig. 4(a), the LDA output, based on the NIRS signal through time, is depicted. As mentioned earlier, a change in curvature implies a change of the mental state (i.e., from active to idle or from idle to active). The blue patches indicate an active state, estimated from the NIRS data. In the lower part of Fig. 4(a), the estimated mental states are depicted as binary numbers (activation function).

Fig. 4(b) explains how the type I is working. The yellow line is continuous EEG classifier output (p_4^k: discriminating between the two classes: left vs. right). When the activation function indicates an active state, the EEG classifier (p_4^k) is decided to the current class. Whereas, when the activation function indicates an inactive state, the current state is decided to the idle class. All the small squares depict the outcomes of the classification result by each type of classifier ensemble ($[-1, 0, 1]$, corresponding to right, idle, and left class). Correctly classified boxes are colored in black, while red boxes indicate misclassification. The red and green patches indicate the label of true active classes (red: right hand imagery, green: left hand imagery) as well as their duration.

Fig. 4(d) shows the OVR-outputs of the three EEG-based classifiers ($p_{1,2,3}^k$). The classifier with the maximum output determines

the current mental state. Fig. 4(c) shows the same three EEG-based OVR classifier outputs as in Fig. 4(d), with the following difference: when an active state was detected by the NIRS-based activation function, the outputs of the active classes (red line: left vs. others, green line: right vs. others) received increased weight ($p'^{k}_{1,2}$). Similarly, when an idle state was detected, the idle state EEG-based classifier (blue line) received increased weight (p'^{k}_{3}). The original EEG-based OVR classifier outputs are also plotted as a dotted line for easy comparison.

2.2.6. Performance evaluation

The pseudo-online evaluation was validated by 4-fold chronological cross-validation. In the first fold the first half of the data was used as the training set, while the second half of the data was further split into equal halves, being validation and test set. The further folds of the cross-validation scheme were such that the test set covered the whole range of the data once.

For the performance evaluation of an asynchronous BCIs [33], the accuracy, sensitivity, specificity, and AUC scores, which is the area under the ROC (Receiver operator Characteristics) curve were calculated. The correct estimation of right and left hand movement imagery classes was considered the true positive, and the correct estimate of the idle state was considered the true negative. The Wilcoxon rank-sum test (significant level: $p < 0.05$) was computed to examine the performance improvement between uni-modal EEG and proposed multi-modal EEG–NIRS system for all evaluation parameters of accuracy, sensitivity, specificity and AUC score.

For the successful control of a BCI system, a minimum accuracy of 70% has previously been proposed [34]. Subjects with less than 70% are commonly referred to as 'illiteracy' and this group of subjects is a non-negligible portion of users (estimated 15–30%) [35]. In our study, to examine the effects of our multi-modal setup on this illiterate group of subjects, we thresholded the performance at 0.7 AUC on a subject level and thus created an 'illiteracy group' as well as a 'normal group'.

3. Results

Our first goal is to show that the proposed subject-dependent classifier strategies improve the classification accuracy of the idle-state detection for BCI systems.

All binary, uni-modal classifiers that are necessary for the ensemble learning were first evaluated in a synchronous fashion and their classification accuracies (%) can be obtained from Table 1. The left part of the table shows results for EEG, while the right part for NIRS. Individual NIRS chromophores (HbO and HbR) were considered individually as well as their combination by simple concatenation of features. Results of the concatenated features outperformed individual ones. While this result was not significant, for future analysis only the combination of features was used.

Table 2 shows classification accuracies for EEG as well as the combination of EEG and NIRS, based on a pseudo-online approach (see Section 2.2.3). The left part of the figure considers uni-modal EEG, while the right part shows results for the proposed EEG+NIRS ensemble classifier. As explained in Section 2.2.2 two analysis methods for the validation of EEG features were used, termed 'CSP' and 'BSSFO'. As can be seen in the averages, the BSSFO approach outperforms the CSP method for uni-modal EEG-based classification.

The performance of the two types of ensemble classifiers (introduced in Section 2.2.5) was evaluated on the validation data and then applied to the test data. The selected type is given in the last column of the table. The proposed hybrid pseudo-online BCI outperformed the EEG stand-alone system, regardless of which EEG analysis method was chosen. All performance parameters (accuracy, sensitivity, specificity, and AUC score) are evaluated

Table 2
Classification accuracy (Acc), sensitivity (Sen), specificity (Spec) and AUC (all in %) for individual subjects as well as their mean, comparing uni-modal EEG as well as multi-modal EEG+NIRS. Two different spatio-temporal analysis methods are compared: classical CSP and a more recent method, BSSFO. T indicates type.

Subj	EEG				EEG+NIRS				
	Acc	Sen	Spec	AUC	Acc	Sen	Spec	AUC	T
CSP									
a	54.1	40.0	60.3	0.63	59.8	78.2	55.8	0.79	I
b	69.3	70.3	69.2	0.76	69.0	70.8	68.6	0.76	II
c	40.0	65.1	33.7	0.57	44.7	59.2	41.2	0.59	II
d	59.1	63.5	58.4	0.69	67.3	64.9	68.3	0.75	II
e	61.1	67.4	59.7	0.74	59.7	75.3	55.7	0.75	II
f	43.1	58.2	39.8	0.59	43.5	59.0	40.0	0.59	II
g	68.7	62.7	70.4	0.76	68.0	73.9	66.3	0.79	II
h	63.4	57.8	65.5	0.68	63.9	63.8	63.8	0.71	II
i	42.4	38.8	43.9	0.51	50.5	50.5	50.5	0.60	I
j	53.7	46.5	57.7	0.58	57.6	62.6	55.9	0.66	I
k	36.3	67.0	28.4	0.54	62.0	85.0	55.9	0.78	I
l	56.3	49.3	60.0	0.62	56.1	67.7	52.8	0.68	I
m	50.5	52.1	49.8	0.63	57.1	62.0	55.7	0.71	II
n	64.8	52.4	70.2	0.65	71.3	73.3	70.5	0.78	II
Mean	54.5	56.5	54.8	0.64	59.3[a]	67.6[b]	57.2	0.71[b]	
BSSFO									
a	72.9	54.4	78.7	0.80	65.2	78.2	62.2	0.81	I
b	68.6	69.5	68.6	0.75	68.6	70.3	68.2	0.75	II
c	61.6	56.0	63.4	0.72	61.6	58.1	62.7	0.73	II
d	65.1	52.9	69.3	0.70	67.0	64.4	68.0	0.75	I
e	61.8	71.3	59.3	0.75	60.9	76.9	56.9	0.76	II
f	48.3	64.9	44.6	0.64	48.7	66.3	44.8	0.65	II
g	68.7	62.7	70.4	0.76	68.0	73.9	66.3	0.79	II
h	66.5	68.4	65.8	0.74	66.0	71.8	63.9	0.75	II
i	39.5	49.7	37.2	0.55	48.1	44.6	49.1	0.60	II
j	41.0	68.2	33.6	0.54	54.3	64.7	50.9	0.64	II
k	33.5	73.6	24.8	0.54	61.7	84.3	55.9	0.78	I
l	56.0	47.1	60.2	0.62	56.2	66.7	53.2	0.69	II
m	63.8	51.9	67.2	0.73	61.8	62.9	61.6	0.75	II
n	61.4	58.3	62.5	0.65	70.4	71.9	69.8	0.77	II
Mean	57.7	60.6	57.7	0.68	61.3	68.2[b]	59.5	0.73[b]	

[a] Indicates $p < 0.05$.
[b] Indicates $p < 0.01$.

across all subjects for CSP as well as BSSFO. Wilcoxon signed rank tests yield significant performance increases for the accuracy, sensitivity and AUC scores for CSP ($p=0.013$, $p=0.0009$ and $p=0.0002$, respectively) as well as sensitivity and AUC scores for BSSFO ($p=0.029$ and $p=0.0004$, respectively). However, specificity of CSP ($p=0.062$) as well as accuracy and specificity of BSSFO ($p=0.35$ and $p=0.85$, respectively) did not reach significant levels. Performance of uni-modal NIRS was also evaluated in pseudo-online fashion and the results can be seen in Table 3. NIRS performs poorly in the pseudo-online setting. All considered performance measures are significantly worse, when compared to uni-modal EEG ($p=0.003$, $p=0.013$, $p=0.041$ and $p=0.0001$) as well as to the multi-modal EEG+NIRS ($p=0.0001$, $p=0.002$, $p=0.011$ and $p=0.0001$) setup.

The scatter plots in Fig. 5 compare AUC scores for uni-modal EEG (x-axis) with the two proposed types of multi-modal classifier combinations (y-axis). Dots above the green line indicate that a subject's performance has increased because of the additional information provided by the NIRS signal as compared to the EEG signal alone. The percentage of the subjects for whom the combination led to an equal or improved decoding is shown on the top left of each plot. Furthermore, p-values resulting from a Wilcoxon signed rank test are shown at the bottom right. Illiterate subjects (≤ 0.7 AUC on the validation set) are marked with a star (also see Fig. 7). Type I combination shows high variability of performance, i.e. adding the NIRS information can be both helpful and harmful

Table 3
Shows classification accuracy (Acc), sensitivity (Sen), specificity (Spec) and AUC scores for uni-modal NIRS.

Subject	NIRS			
	Acc	Sen	Spec	AUC
a	36.2	38.2	37.9	0.45
b	39.3	37.2	44.1	0.47
c	37.2	49.8	40.0	0.50
d	40.6	21.3	49.4	0.43
e	31.0	56.6	23.6	0.49
f	21.6	74.8	7.4	0.46
g	39.3	12.2	50.3	0.44
h	25.4	67.9	14.4	0.48
i	45.8	19.1	60.2	0.46
j	21.2	69.4	10.6	0.47
k	38.7	35.2	44.0	0.46
l	45.1	15.7	59.8	0.45
m	55.1	3.8	77.3	0.48
n	35.9	25.0	39.7	0.45
Mean	36.6	37.6	39.9	0.46

depending on the subject. For subjects with low EEG performance adding NIRS generally increases the performance. For the type I combination only half of the subjects show increased AUC scores. In contrast, type II shows an overall increased performance for all of subjects (EEG-CSP), and for 13 out of 14 subjects (EEG-BSSFO). These increases are highly significant ($p=0.0001$ and $p=0.0004$, respectively).

Fig. 6 shows the delays of idle state detection for various considered methods. The upper part of the figure shows averaged LDA classifier outputs for NIRS, while the lower part shows averaged EEG classifier outputs. The blue lines indicate binary classifier outputs of idle vs. active classes. The red lines indicate an average of classifiers, decoding active classes: given the active class label of the cue, 'left vs. others' or 'right vs. others' classifier outputs were considered for the average. At time 0 s an active state is cued, which lasts for 4 s, followed by an idle state of 10.5 ± 1.5 s, which can be obtained from the first line of blue (A) and gray boxes (I) in the center, the true label. NIRS-AF, NIRS-OVR and EEG-OVR indicate the average predictions of active and idle states for these three considered methods. While NIRS-AF considers the inflection

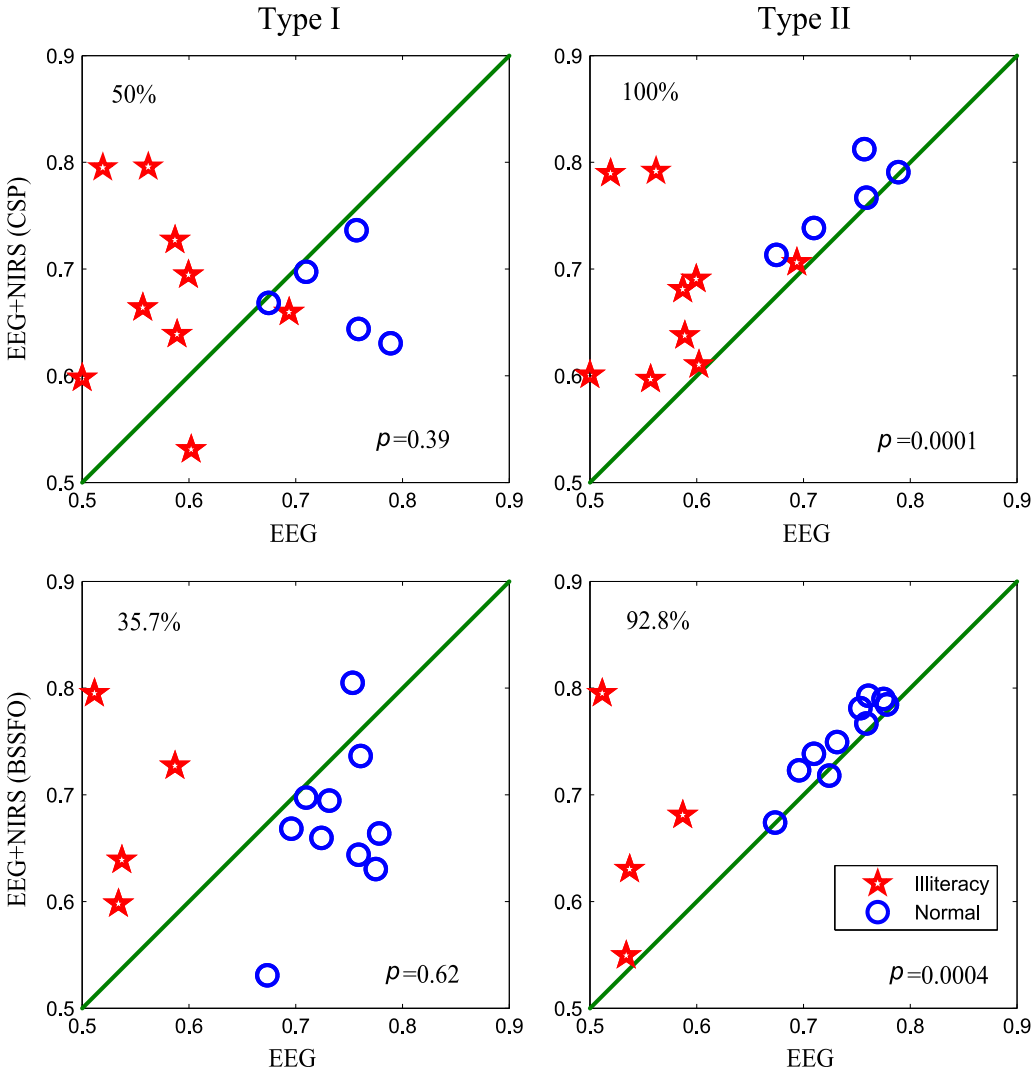

Fig. 5. Scatter plot comparing AUC scores and significant values of various combination of NIRS and EEG. The *x*-axis depicts the EEG-AUC score. The *y*-axis depicts the AUC scores of the EEG+NIRS combination. (For interpretation of the references to color in the text, the reader is referred to the web version of this paper.)

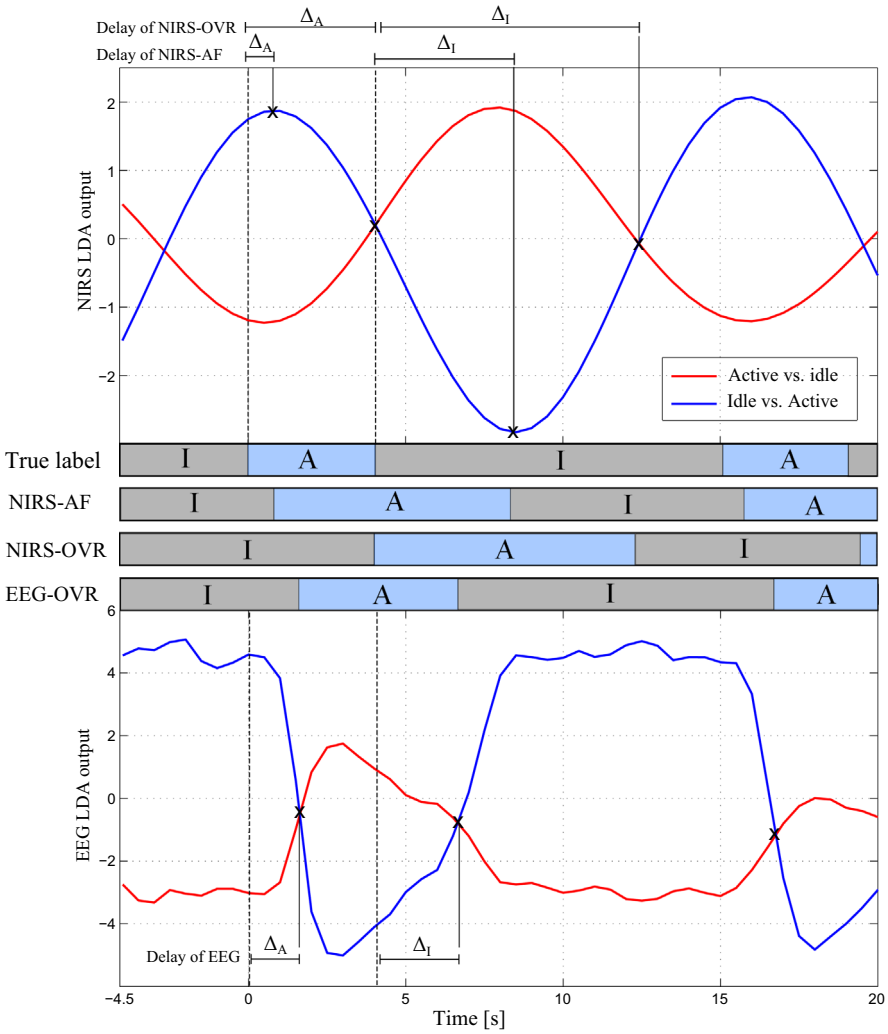

Fig. 6. Shows average LDA outputs for two NIRS classifiers (top) as well as two EEG classifiers (bottom). Red lines indicate active classes (left and right hand imagery) versus idle states. At time 0 s an active state is cued, which lasts for 4 s, followed by an idle state of 10.5 ± 1.5 s, which can be obtained from the first line of blue (A) and gray boxes (I) in the center. NIRS-AF, NIRS-OVR and EEG-OVR indicate the average predictions of active and idle state for these three methods. Δ_A and Δ_I indicate the delays of active and idle state detection, respectively. (For interpretation of the references to color in this figure caption, the reader is referred to the web version of this paper.)

points of the 'idle vs. active' classifier (see Section 2.2.4), NIRS-OVR and EEG-OVR are based on a winner-takes-all approach. The average time delay for the detection of idle-state onset across subjects is 1.25 ($\pm$0.82) for NIRS-AF, 4.07 ($\pm$0.97) for NIRS-OVR and 1.39 ($\pm$0.28) for EEG-OVR. The offset values are 4.45 ($\pm$1.13) for NIRS-AF, 8.44 ($\pm$0.81) for NIRS-OVR and 3.18 ($\pm$(0.79) for EEG-OVR. The delay of the idle state detection with the NIRS-AF method is significantly shortened, when compared to NIRS-OVR ($p=0.0003$).

Fig. 7 shows the classification performances of individual subjects with respect to changing the weight-parameter θ. While for the earlier analysis the optimal θ was chosen with the help of the validation set (as explained in Section 2.2.5), here we examine the performance changes, with respect to varying θ. When the weight-parameter θ is 0, three OVR-based stand-alone EEG classifiers are used to decode. By increasing the weight-parameter θ the contribution of NIRS is also increased. Therefore, the weight-parameter θ decides how heavily the hybrid system depends on the NIRS signal. Here, we divide the 14 subjects into two groups, based on their EEG performance. Subjects with an AUC score of above 0.70 belong to the *normal group*, while subjects with a lower BCI performance (AUC score $\leq$ 0.70) belong to the *illiteracy group*. The *illiteracy group* shows an overall increased performance, when adding the NIRS information. However, the *normal group* shows a decrease in their performance after increasing the weight of the NIRS signal (i.e. by increasing θ). This trend can be seen for both considered EEG analysis methods (CSP and BSSFO).

To further examine the effects of the multi-modal combination on the illiterate and normal groups, the performance changes of these two groups are shown in Fig. 8. While the normal group shows similar accuracy, the illiteracy group shows an increase for all considered performance measures. Sensitivity and AUC scores are significantly enhanced ($p=0.011$ and $p=0.003$, respectively) for the multi-modal setup.

4. Discussion and conclusion

To stabilize the performance of pseudo-online BCIs, we introduced a multi-modal hybrid BCI. It shows that for some subjects a single modality is not capable of estimating mental states reliably enough for the robust control of BCIs. Nevertheless, the use of NIRS as one of the modalities suffers from a temporal lag because of the hemodynamic peak between 4 s and 7 s after stimulus onset. Therefore, we proposed an activation function (*active vs. idle state detection*), which uses the curvature of NIRS classifier outputs. The experimental results indicate that the binary activation function is fairly synchronized with stimulus onset time points (Fig. 4(a)).

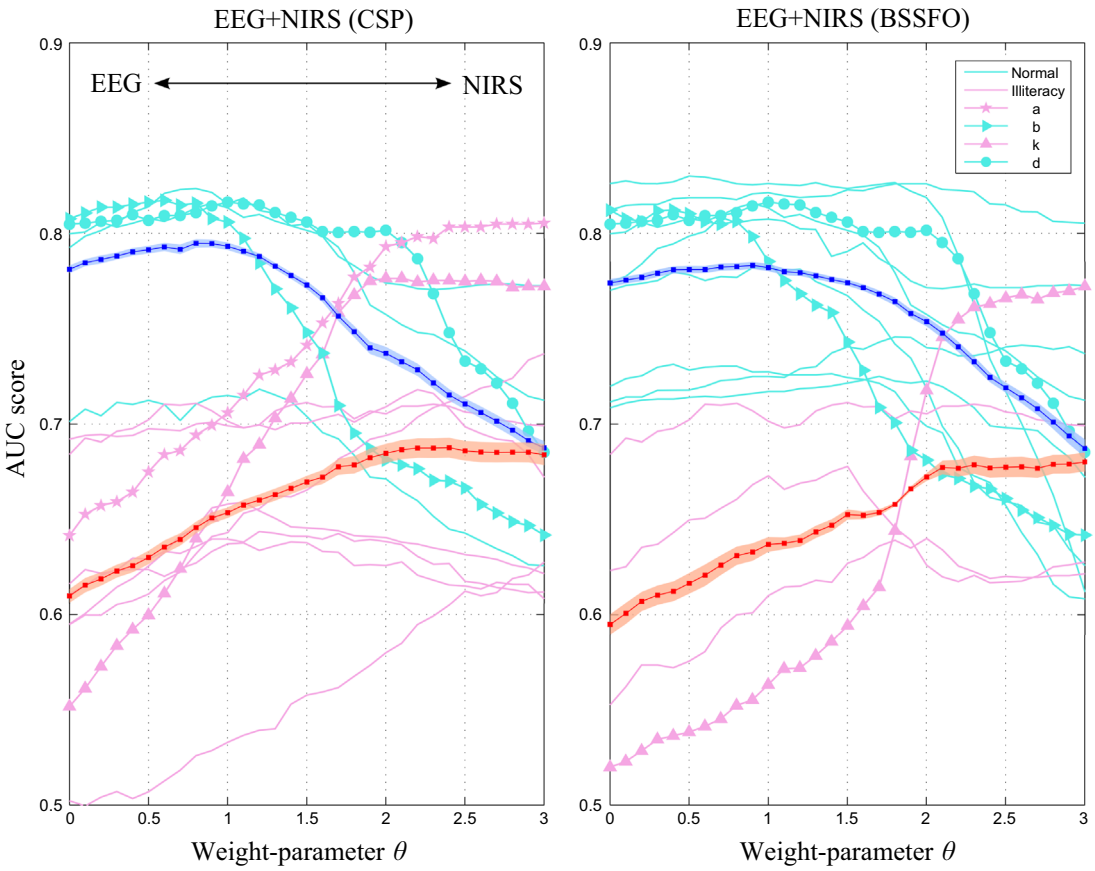

Fig. 7. Performance evaluation by change of weight-parameter θ in the validation procedure. The x-axis depicts the weight-parameter θ. The y-axis depicts the AUC score. Bold blue and red lines depict the mean performance of *normal* and *illiteracy* groups with variance (bounded line). (For interpretation of the references to color in this figure caption, the reader is referred to the web version of this paper.)

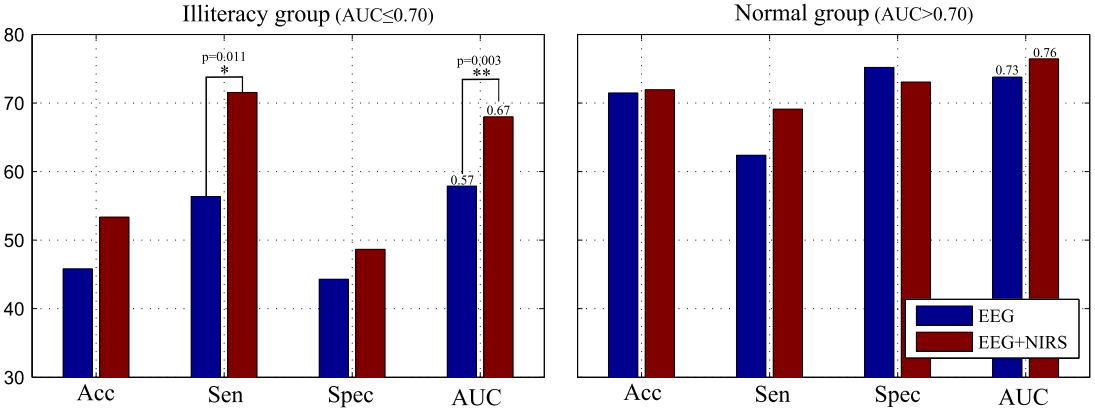

Fig. 8. Compares performance measures for illiteracy and normal groups. The blue (illiteracy group) and red (normal group) bars indicate the mean of accuracy, sensitivity, specificity and AUC score. (For interpretation of the references to color in this figure caption, the reader is referred to the web version of this paper.)

Pfurtscheller et al. introduced the concept of a *brain-switch* [12], which relies on a hybrid BCI. Here one of the modalities (e.g. NIRS) is responsible for activating the BCI, while another modality is responsible for active-state decoding. This asynchronous hybrid BCI combines a NIRS BCI with EEG-based SSVEP orthosis control. The SSVEP is activated when the relative oxyhemoglobin concentration change exceeds a subject-specific threshold. Khan et al. suggest a hybrid EEG–NIRS setup to decode four movement directions [36]. NIRS optodes are positioned over the prefrontal cortex, while EEG electrodes are positioned over the left and right motor cortical regions. Two movement directions are controlled by NIRS and the two remaining ones by EEG. Unimodal classification is performed by LDA, and evaluated individually. Fazli et al. employed a meta-classifier to combine classifier outputs from NIRS and EEG [14]. In our approach we propose two types of classification strategies. For both types we estimate a NIRS-based classifier, which detects the idle/active state, and is based on the derivative of the NIRS classifier output. Depending on this output an active-state EEG-based classifier is weighted accordingly.

We observe that in our study several subjects failed to perform in either one of the modalities. Therefore, two alternative approaches of subject-dependent classification strategies are suggested that use complementary information content inferred from each of the modalities. The first approach (type I) shows the significantly

enhanced performance for some subjects by reducing the classification problem from three classes (idle, left, and right motor imagery) to two steps of binary decisions. The second approach (type II) is to weigh the EEG-classifier outputs using the NIRS activation function. The weight-parameter θ thereby determines the dependence between the EEG and NIRS modalities. When the NIRS-based activation function does not classify the active and the idle mental state correctly, only a small weight-parameter θ is chosen, which sparsely affects the EEG classifier output. Therefore, classification performance of the second approach will rarely exhibit major drops in performance as compared to uni-modal EEG classification (Fig. 5). Therefore the second approach is more flexible in its capability to reduce the risk of one modality not functioning properly.

Tomita et al. [37] proposed an SSVEP paradigm using simultaneous recordings of EEG and NIRS. The idle-state is decoded by the NIRS and derivatives of NIRS signals are used to reduce the hemodynamic delay. They find that derivatives are positive in most regions during the "*ON-period*", and vice versa for the "*OFF-period*". Their approach is similar to ours in the sense that they find NIRS signals to be valuable for idle-state detection and that derivatives are useful for reducing the latency of the hemodynamic response. Here we considered an SMR-based paradigm and investigate which multi-modal combination is superior for idle-state detection. Our results for uni- and multimodal feature combinations indicate that combining NIRS with EEG leads to increased accuracy (see Tables 2 and 3). Furthermore, we also show that NIRS signals are not only useful for on–off control (i.e., active/idle state detection), but can also contribute to the classification of active classes, confirming earlier results [14].

While some previous hybrid BCI approaches relied on two paradigms [12,37], here we consider only a single paradigm, which is evaluated within a multi-modal setup. This approach may simplify the operation of the BCI on the user side. By employing a hybrid-BCI approach, the overall performance was significantly enhanced and some subjects showed remarkably improved accuracies. However, the analyzing routines presented here have been solely validated in an offline fashion using pseudo-online technique. Our future work will extend our research to a real-time asynchronous hybrid BCI with visual feedback.

Conflict of interest

None declared.

Acknowledgements

This work was supported by National Research Foundation of Korea (NRF) grant funded by the Korea government (No. 2012-005741).

References

[1] M.-H. Lee, S. Fazli, J. Mehnert, S.-W. Lee, Improving the performance of brain–computer interface using multi-modal neuroimaging, in: Proceedings of the 2nd IEEE Asian Conference on Pattern Recognition, Okinawa, Japan, 2013, pp. 511–515.
[2] G. Dornhege, Toward Brain–Computer Interfacing, The MIT Press, Cambridge, 2007.
[3] D. van de Ville, S.-W. Lee, Brain decoding: opportunities and challenges for pattern recognition, Pattern Recognit. 45 (6) (2012) 2033–2034.
[4] F. Galán, M. Nuttin, E. Lew, P.W. Ferrez, G. Vanacker, J. Philips, J.d.R. Millán, A brain-actuated wheelchair: asynchronous and non-invasive brain–computer interfaces for continuous control of robots, Clin. Neurophysiol. 119 (9) (2008) 2159–2169.
[5] G. Pfurtscheller, C. Neuper, G. Muller, B. Obermaier, G. Krausz, A. Schlogl, R. Scherer, B. Graimann, C. Keinrath, D. Skliris, et al., Graz-BCI: state of the art and clinical applications, IEEE Trans. Neural Syst. Rehabil. Eng. 11 (2) (2003) 1–4.
[6] S.D. Power, A. Kushki, T. Chau, Towards a system-paced near-infrared spectroscopy brain–computer interface: differentiating prefrontal activity due to mental arithmetic and mental singing from the no-control state, J. Neural Eng. 8 (6) (2011) 066004.
[7] D. Zhang, Y. Wang, X. Gao, B. Hong, S. Gao, An algorithm for idle-state detection in motor-imagery-based brain–computer interface, Comput. Intell. Neurosci. 2007 (2007) 5.
[8] J. del R. Millán, J. Mouriño, Asynchronous BCI and local neural classifiers: an overview of the adaptive brain interface project, IEEE Trans. Neural Syst. Rehabil. Eng. 11 (2) (2003) 159–161.
[9] K.K. Ang, Z.Y. Chin, H. Zhang, C. Guan, Mutual information-based selection of optimal spatial-temporal patterns for single-trial EEG-based BCIs, Pattern Recognit. 45 (6) (2012) 2137–2144.
[10] A. Tzovara, M.M. Murray, G. Plomp, M.H. Herzog, C.M. Michel, M. de Lucia, Decoding stimulus-related information from single-trial EEG responses based on voltage topographies, Pattern Recognit. 45 (6) (2012) 2109–2122.
[11] S.-K. Yeom, H.-I. Suk, S.-W. Lee, Person authentication from neural activity of face-specific visual self-representation, Pattern Recognit. 46 (4) (2013) 1159–1169.
[12] G. Pfurtscheller, B.Z. Allison, G. Bauernfeind, C. Brunner, T. Solis Escalante, R. Scherer, T.O. Zander, G. Müller-Putz, C. Neuper, N. Birbaumer, The hybrid BCI, Front. Neurosci. 4 (2010) 3.
[13] S. Fazli, S.-W. Lee, Brain computer interfacing: a multi-modal perspective, J. Comput. Sci. Eng. 7 (2) (2013) 132–138.
[14] S. Fazli, J. Mehnert, J. Steinbrink, G. Curio, A. Villringer, K.-R. Müller, B. Blankertz, Enhanced performance by a hybrid NIRS–EEG brain computer interface, NeuroImage 59 (1) (2012) 519–529.
[15] K.K. Kwong, J.W. Belliveau, D.A. Chesler, I.E. Goldberg, R.M. Weisskoff, B.P. Poncelet, D.N. Kennedy, B.E. Hoppel, M.S. Cohen, R. Turner, Dynamic magnetic resonance imaging of human brain activity during primary sensory stimulation, Proc. Natl. Acad. Sci. 89 (12) (1992) 5675–5679.
[16] Z. Saad, K. Ropella, R. Cox, E. DeYoe, Analysis and use of fMRI response delays, Hum. Brain Mapp. 13 (2) (2001) 74–93.
[17] R. Sitaram, H. Zhang, C. Guan, M. Thulasidas, Y. Hoshi, A. Ishikawa, K. Shimizu, N. Birbaumer, Temporal classification of multichannel near-infrared spectroscopy signals of motor imagery for developing a brain–computer interface, NeuroImage 34 (4) (2007) 1416–1427.
[18] S. Luu, T. Chau, Decoding subjective preference from single-trial near-infrared spectroscopy signals, J. Neural Eng. 6 (1) (2009) 016003.
[19] S.G. Mason, G.E. Birch, A brain-controlled switch for asynchronous control applications, IEEE Trans. Biomed. Eng. 47 (10) (2000) 1297–1307.
[20] F. Bießmann, S.M. Plis, F.C. Meinecke, T. Eichele, K.-R. Müller, Analysis of multimodal neuroimaging data, IEEE Rev. Biomed. Eng. 4 (2011) 26–58.
[21] F. Bießmann, F.C. Meinecke, A. Gretton, A. Rauch, G. Rainer, N. Logothetis, K.-R. Müller, Temporal kernel canonical correlation analysis and its application in multimodal neuronal data analysis, Mach. Learn. 79 (1–2) (2009) 5–27.
[22] S. Dähne, F. Bießmann, F.C. Meinecke, J. Mehnert, S. Fazli, K.-R. Müller, Integration of multivariate data streams with bandpower signals, IEEE Trans. Multimed. 15 (5) (2013) 1001–1013.
[23] C. Vidaurre, C. Sannelli, K.-R. Müller, B. Blankertz, Machine-learning-based coadaptive calibration for brain–computer interfaces, Neural Comput. 23 (3) (2011) 791–816.
[24] L. Kocsis, P. Herman, A. Eke, The modified Beer–Lambert law revisited, Phys. Med. Biol. 51 (5) (2006) N91.
[25] B. Blankertz, R. Tomioka, S. Lemm, M. Kawanabe, K.-R. Muller, Optimizing spatial filters for robust EEG single-trial analysis, IEEE Signal Process. Mag. 25 (1) (2008) 41–56.
[26] P. Nunez, R. Srinivasan, A. Westdorp, R. Wijesinghe, D. Tucker, R. Silberstein, P. Cadusch, EEG coherency: I: statistics, reference electrode, volume conduction, Laplacians, cortical imaging, and interpretation at multiple scales, Electroencephalogr. Clin. Neurophysiol. 103 (5) (1997) 499–515.
[27] K. Fukunaga, Introduction to Statistical Pattern Recognition, Academic Press, Boston, 1990.
[28] H.-I. Suk, S.-W. Lee, A novel Bayesian framework for discriminative feature extraction in Brain–Computer Interfaces, IEEE Trans. Pattern Anal. Mach. Intell. 35 (2) (2013) 286–299.
[29] R.A. Fisher, The use of multiple measurements in taxonomic problems, Ann. Eugen. 7 (2) (1936) 179–188.
[30] G. Dornhege, B. Blankertz, G. Curio, K.-R. Muller, Boosting bit rates in noninvasive EEG single-trial classifications by feature combination and multiclass paradigms, IEEE Trans. Biomed. Eng. 51 (6) (2004) 993–1002.
[31] E.L. Allwein, R.E. Schapire, Y. Singer, Reducing multiclass to binary: a unifying approach for margin classifiers, J. Mach. Learn. Res. 1 (2) (2001) 113–141.
[32] B. Blankertz, G. Curio, K.-R. Muller, Classifying single trial EEG: towards brain computer interfacing, in: Advances in Neural Information Processing Systems, vol. 1, 2002, pp. 157–164.
[33] E. Thomas, M. Dyson, M. Clerc, An analysis of performance evaluation for motor-imagery based BCI, J. Neural Eng. 10 (3) (2013) 031001.
[34] N. Neumann, J. Kaiser, B. Kotchoubey, T. Hinterberger, N.P. Birbaumer, Brain–computer communication: self-regulation of slow cortical potentials for verbal communication, Arch. Phys. Med. Rehabil. 82 (11) (2001) 1533–1539.
[35] C. Vidaurre, B. Blankertz, Towards a cure for BCI illiteracy, Brain Topogr. 23 (2) (2010) 194–198.
[36] M.J. Khan, M.J. Hong, K.-S. Hong, Decoding of four movement directions using hybrid nirs-eeg brain–computer interface, Front. Hum. Neurosci. 8 (2014).
[37] Y. Tomita, F.-B. Vialatte, G. Dreyfus, Y. Mitsukura, H. Bakardjian, A. Cichocki, Bimodal BCI using simultaneously NIRS and EEG, IEEE Trans. Biomed. Eng. 61 (4) (2014) 1274–1284.

Min-Ho Lee received the B.S. degree in Computer Science and Engineering from Seokyeong university, Seoul, Korea, in 2012. He is currently a Ph.D. student in the Department of Brain and Cognitive Engineering in Korea University. His research interests include brain–computer interfacing and pattern recognition.

Siamac Fazli received his B.Sc. in Physics from the University of Exeter, his M.Sc. in Medical Neurosciences from Humboldt University Berlin and his Ph.D. degree in Computer Science from the Technical University in Berlin. Currently, he is an Assistant Professor at Korea University, Seoul, South Korea. His research interests include brain–computer interfacing, machine learning, and neuroscience.

Jan Mehnert received his Ph.D. from the Department of Software Engineering and Theoretical Computer Science at the Berlin Institute of Technology, Germany, in 2012. Currently, he is a Post-doctoral fellow at Berlin Institute of Technology and at Charité University Hospital, Berlin, Germany. His research includes near-infrared spectroscopy, multimodal signal processing and brain–computer interfaces.

Seong-Whan Lee is a Hyundai Motor Chair Professor at Korea University, where he is the Head of the Department of Brain and Cognitive Engineering. He received the B.S. degree in computer science and statistics from Seoul National University, Seoul, Korea in 1984, and the M.S. and Ph.D. degrees in computer science from KAIST in 1986 and 1989, respectively. He is a Fellow of the IEEE, IAPR, and Korean Academy of Science and Technology. His research interests include pattern recognition, computer vision, and brain engineering.